

Inhomogeneous hardcore bosonic mixture with checkerboard supersolid phase: Quantum and thermal phase diagram

F. Heydarinasab* and J. Abouie†

Department of Physics, Institute for Advanced Studies in Basic Sciences (IASBS), Zanjan 45137-66731, Iran

(Dated: January 26, 2022)

We introduce an inhomogeneous bosonic mixture composed of two kinds of hardcore and semi-hardcore boson with different nilpotency conditions and demonstrate that in contrast with the standard hardcore Bose Hubbard model, our bosonic mixture with nearest and next nearest neighbor interactions on a square lattice develops the checkerboard supersolid phase characterized by the simultaneous superfluid and checkerboard solid orders. Our bosonic mixture is created from a two-orbital Bose-Hubbard model including two kinds of bosons: a single orbital boson and a two-orbital boson. By mapping the bosonic mixture to an anisotropic inhomogeneous spin model in the presence of a magnetic field, we study the ground state phase diagram of the model by means of cluster mean field theory and linear spin wave theory and show that various phases such as solid, superfluid, supersolid and Mott insulator appear in the phase diagram of the mixture. Competition between the interactions and magnetic field causes the mixture to undergo different kinds of first and second order phase transitions. By studying the behavior of the spin wave excitations we find the reasons of all first and second order phase transitions. We also obtain the temperature phase diagram of the system using cluster mean field theory. We show that the checkerboard supersolid phase persists at finite temperature comparable with the interaction energies of bosons.

PACS numbers: 03.75.-b, 05.30.-d, 67.80.kb

I. INTRODUCTION

Supersolids are characterized by the simultaneous presence of a nontrivial crystalline solid order and superfluid phase order in the context of quantum lattice gas models^{1,2}. Discussing the possibility of supersolidity, has attracted renewed interest in connection with ultracold Bose gases in optical lattices³⁻⁸. The precise controllability of optical lattice systems has motivated theoretical explorations of supersolid phase in various systems, such as one dimensional chains⁹⁻¹², two dimensional square¹³⁻²³, honeycomb^{24,25}, triangular²⁶⁻³⁵ and kagome³⁶ lattice structures, two-dimensional spin-1/2 dimer model with an anisotropic intra-plane anti-ferromagnetic coupling³⁷, bilayer systems of dipolar lattice bosons³⁸ and three dimensional cubic lattice^{17,39-41}. These extensive studies show that no supersolid phases can exist in the ground state phase diagram of the hardcore Bose Hubbard model with nearest neighbor interaction for bipartite lattices^{22-25,42-44}. In these systems, due to the formation of antiphase walls between ordered domains⁴⁵, supersolid states are unstable towards phase separation¹⁵. In order to have stable supersolid phases, one has to modify the model by introducing repulsive dipole-dipole interaction^{19,22,46} where has the role of increasing the energy cost of domain wall formations. Adding next nearest neighbor interaction^{23,42,44,47,48}, correlated hoppings^{21,49}, or treating soft core bosons^{14,15}, two-component Bose-Fermi⁵⁰⁻⁵² and Bose-Bose^{53,54} mixtures, and three component Bose-Bose-Fermi mixture⁵⁵ result also stable supersolids.

In this paper we introduce a different inhomogeneous bosonic model (IBM) which is composed of two kinds of hardcore and semi-hardcore boson, a and b , with *different*

nilpotency conditions: $(a_i^\dagger)^2 = 0$ for a and $(b_i^\dagger)^3 = 0$ for b bosons, and show that the model on a square lattice with nearest neighbor (NN) and next nearest neighbor (NNN) interactions is an appropriate ground for searching various supersolid orders. The nilpotency condition for b bosons signifies that one can put up two b particles on each lattice site. Our IBM is created from a Bose-Hubbard model including two kinds of bosons: a single orbital boson and a two-orbital boson. By mapping the IBM to an anisotropic inhomogeneous spin-(1,1/2) model in the presence of a magnetic field, we study the ground state phase diagram of the model by means of cluster mean field (CMF) theory and linear spin wave (LSW) theory and show that various phases such as solid, superfluid, supersolid and Mott insulator appear in the phase diagram of the mixture. We demonstrate that in contrast with the standard hardcore Bose Hubbard model in which long range hopping terms are required for the superfluidity^{21,49}, or long range dipole-dipole interactions are necessary to suppress quantum fluctuations for the stability of checkerboard supersolid (CSS) order on the square lattice^{18,19,22,46}, our IBM possesses a stable CSS phase even in the absence of long range interaction and long range hopping terms. This stability is attributed to the difference in the nilpotency conditions of a and b bosons. The small amount of spin wave fluctuations also show the stability of the CSS phase. Making use of LSW theory and obtaining the excitation spectra of the IBM, besides the strength of quantum fluctuations around the mean field ground states we find the boundaries of the stability of the mean field phases.

In this paper we also study the effects of temperature on the phase diagram of the system. We obtain the temperature phase diagram of the mixture and show that in

the presence of temperature various phases emerge in the phase diagram. Our results show that the CSS order can persist even at finite temperatures comparable with the interaction energies.

This paper is organized as follows. In section II we introduce our IBM and map the model onto a mixed spin model by making use of hardcore boson-spin transformations. In section III we give a brief review on the CMF theory and generalize the theory to the mixed spin model. By computing the diagonal and off diagonal order parameters we present the CMF ground state phase diagram of the model in section IV. In order to investigate the stability of these phases against quantum fluctuations we compute the order parameters within CMF theory with larger clusters. The strengths of quantum fluctuations for each phase are also obtained by means of LSW theory in section V. In this section we investigate the behavior of the spin wave dispersions at phase transitions to figure out the reason of all first and second order phase transitions in the phase diagram of the IBM. In the second part of the paper, in section VI, we obtain the thermal phase diagram of the model and show that the CSS order survives, at finite temperatures. Finally, we summarize our results and give the concluding remarks in section VII.

II. INHOMOGENEOUS BOSONIC MODEL

Let us consider the two kinds of hardcore and semi-hardcore boson a and b which interact via the Hamiltonian:

$$\begin{aligned}
 H_B = & -t \sum_{\langle i,j \rangle} (a_i^\dagger b_j + b_j^\dagger a_i) + U \sum_i n_i^b n_i^b \\
 & + V_1 \sum_{\langle i,j \rangle} n_i^a n_j^b + V_2 \sum_{\langle\langle i,j \rangle\rangle} (n_i^a n_j^a + n_i^b n_j^b) \\
 & - \sum_i (\mu^a n_i^a + \mu^b n_i^b), \quad (1)
 \end{aligned}$$

where $a_i^\dagger(a_i)$ and $b_j^\dagger(b_j)$ are respectively the creation(annihilation) operators of a and b particles at sites i and j , on a two dimensional (2D) bipartite square lattice. The first term represents a hopping between two nearest neighbor sites $\langle i,j \rangle$ where i and j are the lattice points in subsystems I and II, respectively. U is local Coulomb attraction energy ($U < 0$) between b bosons occupying the same site, V_1 is the interaction energy between a and b bosons, V_2 denotes the interaction between two a or two b bosons, and μ^a and μ^b are chemical potentials. $\langle \dots \rangle$ and $\langle\langle \dots \rangle\rangle$ indicate the summations over nearest and next nearest neighbors on the square lattice, respectively.

The a particles are canonical hardcore bosons and satisfy the canonical commutation relations. The number of these bosons at site i is $n_i^a = a_i^\dagger a_i$, and the nilpotency condition for them is $(a_i^\dagger)^2 = 0$. The b particles are how-

ever semi-hardcore bosons and satisfy the nilpotency condition $(b_i^\dagger)^3 = 0$, which signifies that one can put up two b particles on each lattice site. This uncommon nilpotency condition leads to the following non-canonical algebra (see appendix B, for the detailed calculation):

$$\begin{aligned}
 [b_i, b_j] &= [b_i^\dagger, b_j^\dagger] = 0, \\
 [b_i, b_j^\dagger] &= \delta_{ij}(1 - n_i^b), \quad [n_i^b, b_j^\dagger] = \delta_{ij}b_j^\dagger, \quad (2)
 \end{aligned}$$

where $n_j^b (\neq b_j^\dagger b_j)$ is the number of b bosons which possesses the relation $(n_i^b)^\dagger = n_i^b$.

Since the number operator n^b is not equal to $b^\dagger b$, the Hamiltonian in Eq. (1) does not have the standard form of a Bose Hubbard Hamiltonian. But, as we will show in appendix A, this Hamiltonian is created from an standard two-orbital bosonic Hubbard model (see Eq. (A1) in appendix A) by reducing effective number of degrees of freedom. The three-body constraint of the semi-hardcore bosons b , and consequently their non-canonical statistics algebra arise inevitably from the transformations in Eq. (A2) which are employed for mapping the two-orbital Hamiltonian in Eq. (A1) to the one in Eq. (1). At the first glance it may seem that the non-canonical statistics of b particles makes the model complicated, but as we will show in next sections, using a simple boson-spin transformation, the Hamiltonian (1) maps to an standard spin Hamiltonian with rich phase diagrams.

It is worth to mention that two independent physical properties are responsible for the quantum statistics of particles. The first one is exchange or permutation statistics which concerns braiding of particles and the second one is exclusion statistics which concerns number of particles allowed to occupy the same site⁵⁶. It should be noted that, although the commutation relations in Eq. (2) have fractional exclusion statistics, they obey canonical exchange statistics, and should not be confused with the anyonic particles with fractional exchange statistics^{57–62}. The anyonic algebra can be created and manipulated by using the so-called conditional hopping terms^{63–66} which is not the case in our paper.

Fractional exchange statistics in bosonic systems causes the system to experience different new phases which are not seen in the standard system with canonical bosons. For example, the one dimensional optical lattice of semi hardcore bosons with the constraint $(b_i^\dagger)^3 = 0$ and fractional statistics, proposed by Greschner, *et. al.*⁶⁷, shows a novel two-component superfluid of holon and doublon dimers, characterized by a large but finite compressibility and a multi peaked momentum distribution, which is not seen in the one dimensional canonical model⁶⁸. Moreover, including such an statistics in the dipolar system with hardcore bosons results in an striped supersolid phase⁶⁰. In Eq. (1) we have introduced an inhomogeneous system of hardcore and semi-hardcore bosons which could be realized in a two-orbital bosonic system. The non-canonical statistics of the semi-hardcore bosons causes the model to be mapped to a

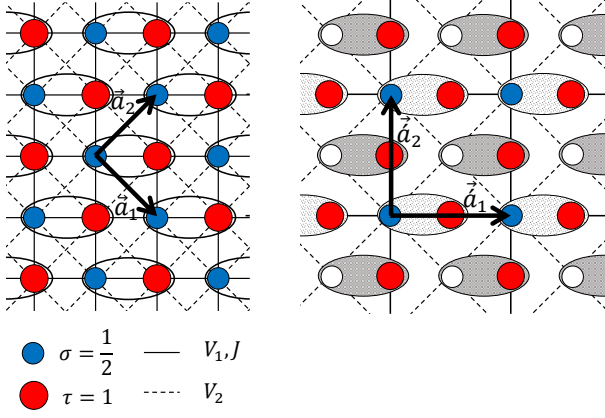


FIG. 1. (Color online) The schematic illustration of a 2D ferrimagnetic spin-(σ, τ) system on square lattice. Left: before the translational symmetry breaking of the Hamiltonian (5), Right: after the translational symmetry breaking in subsystem with spin σ . Each unit cell contains two spins σ and τ . Before symmetry breaking the primitive vectors are \vec{a}_1 and \vec{a}_2 . In the symmetry breaking phase the primitive vectors are $\vec{a}'_1 = \vec{a}_1 + \vec{a}_2$ and $\vec{a}'_2 = \vec{a}_2 - \vec{a}_1$. The right panel shows the checkerboard solid phase in which the translational symmetry of the subsystem with spin σ is broken.

mixed spin model which possesses the CSS phase, in addition to the superfluid, Mott insulating and various solid phases.

Using the Matsubara-Matsuda transformations⁶⁹ for a hardcore bosons:

$$\sigma_i^z = n_i^a - \frac{1}{2}, \quad \sigma_i^+ = a_i^\dagger, \quad \sigma_i^- = a_i, \quad (3)$$

and also the generalized transformations⁵⁶ for b bosons:

$$\tau_j^z = n_j^b - 1, \quad \tau_j^+ = \sqrt{2}b_j^\dagger, \quad \tau_j^- = \sqrt{2}b_j, \quad (4)$$

the Hamiltonian H_B transforms to the following spin Hamiltonian:

$$H = -2J \sum_{\langle i,j \rangle} (\sigma_i^x \tau_j^x + \sigma_i^y \tau_j^y) + U \sum_i (\tau_i^z)^2 + V_1 \sum_{\langle i,j \rangle} \sigma_i^z \tau_j^z + V_2 \sum_{\langle\langle i,j \rangle\rangle} (\sigma_i^z \sigma_j^z + \tau_i^z \tau_j^z) - \sum_i (h^\sigma \sigma_i^z + h^\tau \tau_i^z), \quad (5)$$

with the parameters $J = \sqrt{2}t$, $h^\sigma = \mu^a - 4V_1 - 4V_2$ and $h^\tau = \mu^b - 2U - 2V_1 - 8V_2$. This Hamiltonian is nothing but the frustrated anisotropic mixed spin-(1, 1/2) XXZ model on a bipartite square lattice, with on-site anisotropy, in the presence of longitudinal magnetic fields h^σ and h^τ . Since the hardcore boson-spin transformations (3) and (4) are isomorphic, the symmetries and physical properties of the IBM (1) and the mixed spin Heisenberg model (5) are identically the same. Throughout this paper we consider $h^\sigma = h^\tau = h$, which results the relation $\mu^b - \mu^a = 4V_2 - 2V_1 - 2U$, between the chemical potentials of the two species. A schematic illustration of the ferrimagnetic model (5) is depicted in Fig. 1. The

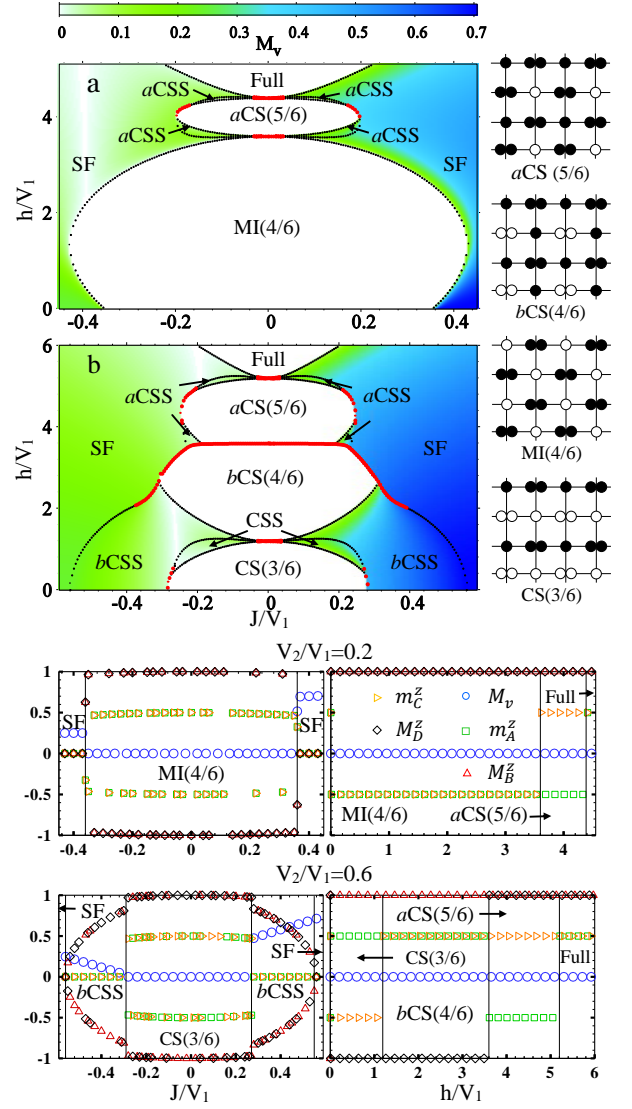


FIG. 2. (Color online) Top (a and b): Ground state phase diagram of the IBM in the absence of U , and for the two different strengths of frustration V_2/V_1 , 0.2 (a) and 0.6 (b). Order parameters are computed using CMF- 2×2 theory. The density of colors shows amount of off diagonal order parameter: $M_v = ((M_T^x)^2 + (M_T^y)^2)^{1/2}$ with $M_T^{x(y)}$, the total magnetization in $x(y)$ direction. The red (black) dotted lines show first(second) order phase transitions. Right: Schematic illustrations of solids and Mott insulator. Different orders are defined as in table I. Bottom: The sublattices longitudinal magnetization and the total transverse magnetization versus J/V_1 at $h = 0$, and versus h/V_1 at $J = 0$.

small (large) filled circles are the spins $\sigma(\tau)$. In the presence of the translational symmetry of the Hamiltonian (5) the primitive vectors are \vec{a}_1 and \vec{a}_2 . When the translational symmetry breaks (at least in one of the subsystems) a phase transition occurs to a checkerboard solid phase in which the lattice structure is given by the primitive translational vectors \vec{a}'_1 and \vec{a}'_2 with four basis. As an example we have illustrated in the right panel of Fig.

1 a checkerboard pattern where the translational symmetry of the subsystem with spin σ is broken.

In anisotropic spin-1/2 models on square lattice with NN and NNN interactions, due to the strength of frustration, quantum fluctuations in spin direction are large enough to destroy the CSS order. In contrast, we will demonstrate that the anisotropic ferrimagnetic spin-(1, 1/2) model in Eq. (5) possesses a stable CSS phase. This is in part due to the fact that each spin-1/2 is surrounded by four spins 1 which causes decreasing of quantum fluctuations. Besides the CSS phase, different solid orders and Mott insulating phase emerge in the phase diagram of the system which are not seen in the homogeneous spin $\frac{1}{2}$ models. In following sections utilizing CMF approach we study the phase diagrams of the model (5) on a square lattice.

III. CLUSTER MEAN FIELD THEORY

CMF theory is an extension of the standard mean field (MF) theory in which "clusters" of multiple sites are used as an approximate system instead of single sites. Treating exactly the interactions within the cluster and including the interaction of spins outside the cluster as an effective field, one can partially take into account fluctuations around classical ground state as well as the effects of correlations of particles. We have generalized the CMF approach of Yamamoto, et al^{22,35,70} which is an extension of Oguchi's method⁷¹ to multiple-sublattice problems, to the inhomogeneous mixed-spin model in Eq. (5). We assume a background with four-sublattice structure (A and C for spins σ , and B and D for spins τ) and embed a cluster of N_C sites into this background. The four-sublattice structure is expected to be emerged due to the NN and NNN interactions. Now, instead of treating the many-body problem in the whole system, we consider the effective cluster Hamiltonian:

$$H_C^{eff} = H_C + \sum_{i \in C} (\vec{h}_i^{eff} \cdot \vec{\sigma}_i + \vec{g}_i^{eff} \cdot \vec{\tau}_i), \quad (6)$$

where the interaction within cluster is given by H_C , the Hamiltonian in Eq. (5) with $i, j \in C$, while the interactions of spins inside the cluster with the rest of the system are included via the effective fields:

$$\begin{aligned} \vec{h}_i^{eff} &= \sum_{\langle i, j \rangle, j \in \bar{C}} [-2J(M_j^x \hat{x} + M_j^y \hat{y}) + V_1 M_j^z \hat{z}] \\ &\quad + V_2 \sum_{\langle \langle i, j \rangle \rangle, j \in \bar{C}} m_j^z \hat{z}, \\ \vec{g}_i^{eff} &= \sum_{\langle i, j \rangle, j \in \bar{C}} [-2J(m_j^x \hat{x} + m_j^y \hat{y}) + V_1 m_j^z \hat{z}] \\ &\quad + V_2 \sum_{\langle \langle i, j \rangle \rangle, j \in \bar{C}} M_j^z \hat{z}, \end{aligned} \quad (7)$$

with \bar{C} part of the system outside the cluster. The magnetizations $\vec{m}_j (= \langle \vec{\sigma}_j \rangle_{CMF})$ and $\vec{M}_j (= \langle \vec{\tau}_j \rangle_{CMF})$ are the

expectation values within the CMF method which act as mean fields on the spins σ and τ . The order parameters $m_j^{x,y,z}$ and $M_j^{x,y,z}$ are calculated self-consistently as the expectation values of the spins inside the cluster. This method reduces to the conventional MF theory for $N_C^\tau = N_C^\sigma = 1$ and becomes exact in the limit of $N_C \rightarrow \infty$.

IV. GROUND STATE PHASE DIAGRAM

According to the relations between the sublattices magnetizations various kinds of solid and supersolid orders are observed in the ground state phase diagram of the IBM (See Fig. 2 for $U = 0$ and Fig. 5 for $U = -1.4V_1$).

In the absence of magnetic field, at $h = 0$, for large values of hopping energy $|J|$ and any strength of frustration, the IBM is in a superfluid (SF) phase where the U(1) symmetry of both subsystems is broken and each boson is spread out over the entire lattice, with long range phase coherence. By decreasing $|J|$ the IBM however, behaves differently for strong and weak frustrations (see Fig. 2, bottom panels, the behavior of the sublattices longitudinal magnetizations versus J/V_1 at $h = 0$). For $V_2/V_1 < 0.4$, at the first order transition line: $V_2 \approx -2.02J + 0.77V_1$ (not shown) the off diagonal long range order are suddenly destroyed and a quantum phase transition occurs from SF to the MI(4/6) Mott insulating phase where both the U(1) and the translational symmetries are preserved. In this phase the average number of bosons in each unit cell is 4/6. Increasing V_2/V_1 , destroys this Mott insulating phase. For $V_2/V_1 \geq 0.4$, by decreasing $|J|$ the translational symmetry of the subsystem b also breaks and a phase transition from SF to the b CSS supersolid phase occurs at the first order transition line: $V_2 \approx 1.53J + 0.07V_1$, where the checkerboard solid order emerges in the subsystem b in addition to the off-diagonal one (see table I for the definition of supersolid phases). By further decreasing of $|J|$, the off diagonal order disappears at the transition line: $V_2 \approx 1.92J + 0.06V_1$, and the translational symmetry of subsystem a also breaks and the mixture enters the CS(3/6) solid phase. In this phase the spins 1 as well as the spins 1/2 are antiparallel and the average number of bosons on each unit cell is 3/6.

In the presence of magnetic field, for $h \neq 0$, depending on the strength of frustration, various kinds of solid order appear in the phase diagram of the IBM. We have plotted in Fig. 2 the phase diagram of the mixture for the two strengths of frustration, $V_2/V_1 = 0.2$ and 0.6. For the weak frustration $V_2/V_1 = 0.2$, in a symmetric region around $J = 0$, at small and moderate magnetic fields the system prefers to be in the MI(4/6) phase. By increasing the magnetic field, the translational symmetry of the subsystem a is broken and the spins 1/2 on one of the sublattices A or C flip in the direction of the magnetic field and the mixture enters the a CS(5/6) solid phase (For the definitions of solid orders, see table I and

TABLE I. Definitions of various orders. TS is the abbreviation of the translational symmetry of the Hamiltonian.

Phases	Order parameters		broken symmetries	
	sublattices magnetizations	total magnetization M_v	subsystem a	subsystem b
SF	$m_A^z = m_C^z, M_B^z = M_D^z$	$\neq 0$	U(1)	U(1)
MI(4/6)	$m_A^z = m_C^z, M_B^z = M_D^z$	0	-	-
Full	$m_A^z = m_C^z = 1/2, M_B^z = M_D^z = 1$	0	-	-
a CS(5/6)	$m_A^z = -m_C^z, M_B^z = M_D^z$	0	TS	-
b CS(4/6)	$m_A^z = m_C^z, M_B^z = -M_D^z$	0	-	TS
CS(3/6)	$m_A^z = -m_C^z, M_B^z = -M_D^z$	0	TS	TS
a CSS	$m_A^z \neq m_C^z, M_B^z = M_D^z$	$\neq 0$	TS, U(1)	U(1)
b CSS	$m_A^z = m_C^z, M_B^z \neq M_D^z$	$\neq 0$	U(1)	TS, U(1)
CSS	$m_A^z \neq m_C^z \neq M_B^z \neq M_D^z$	$\neq 0$	TS, U(1)	TS, U(1)

the schematic pictures in the right column of Fig. 2). In this phase the average number of bosons on each unit cell is 5/6. By increasing V_2/V_1 , the antiferromagnetic V_2 interactions try to make the spins 1 antiparallel as well as spins 1/2. For $V_2/V_1 = 0.6$ around $J = 0$, the translational symmetry of both subsystems breaks and the CS(3/6) solid order emerges in the system. By increasing the magnetic field, the translational symmetry of the subsystem a is restored and a phase transition occurs to the b CS(4/6) where the average number of bosons on each unit cell is 4/6. By further increasing of the magnetic field, the a CS(5/6) solid also appears in the phase diagram of the model just below the saturation field. As the solid phases possess different broken symmetries, we expect the transitions between solid phases to be first order which are illustrated with red dotted lines in the phase diagrams.

Besides the superfluid, solids and Mott insulator, various supersolids also appear in the phase diagram of the mixture (see the definition of supersolid orders in table I). For the whole range of V_2/V_1 , in the two narrow regions on the top and bottom sides of the a CS(5/6) solid phase, the spins tend to lie in the plane perpendicular to the magnetic field. In these regions, the system exhibits the a CSS supersolid phase in which both diagonal (solid a CS(4/6)) and off diagonal long range orders coexist in the system. Increasing the hopping parameter $|J|$, the translational symmetry of the subsystem a restores and the a CS(5/6) solid order disappears where a phase transition occurs from a CSS to the SF phase. For larger values of V_2/V_1 , two other supersolid orders, the b CSS and the CSS phases, also appear in the phase diagram at small magnetic fields around the CS(3/6) solid phase (see Fig. 2-b). Phase transitions from the a CSS and b CSS to the SF are of first or second order, depending on the values of h and $|J|$. All these first and second order phase transitions, are attributed to the behavior of the low energy spin wave excitation which will be discussed in section V.

In order to see the effects of quantum fluctuations we investigate the behavior of both the diagonal and off diagonal order parameters considering clusters with larger sizes in CMF theory. Employing clusters of 8 spins (CMF- 2×4), we have computed the sublattices longitu-

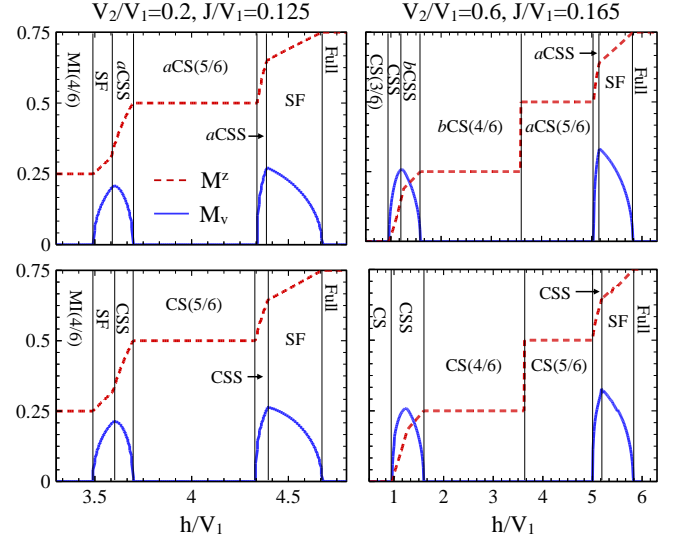


FIG. 3. Diagonal and off diagonal order parameters, computed using CMF theory with 2×2 (top) and 2×4 (bottom) clusters, for the two different strengths of frustration: $V_2/V_1 = 0.2$ and 0.6 , and the two values of hopping parameter: $J/V_1 = 0.125$ and 0.165 where all phases appear in the phase diagram by increasing h . According to the CMF- 2×4 results, quantum fluctuations convert the a CSS and b CSS phases into the CSS phase. The CSS, SF and MI(4/6) phases are not changed by quantum fluctuations.

dinal and transverse magnetizations for different values of h and J . We found out that the quantum fluctuations convert the a CSS and b CSS phases to the CSS phase. Actually, competition between NN and NNN interactions causes the a CS(5/6) and b CS(4/6) solids transform respectively to the CS(5/6) and CS(4/6) solids in which there is no relation between the sublattices longitudinal magnetizations, but the occupation number of each unit cell is conserved. These effects are clearly seen in Fig. 3-bottom, in the behavior of the total magnetizations for $V_2/V_1 = 0.2$ at line $J/V_1 = 0.125$, and for $V_2/V_1 = 0.6$ at line $J/V_1 = 0.165$, where all kinds of orders appear in the system by increasing h . The MI(4/6) insulator and the CSS supersolid are however stable and quantum fluctuations cannot destroy these orders. This is in con-

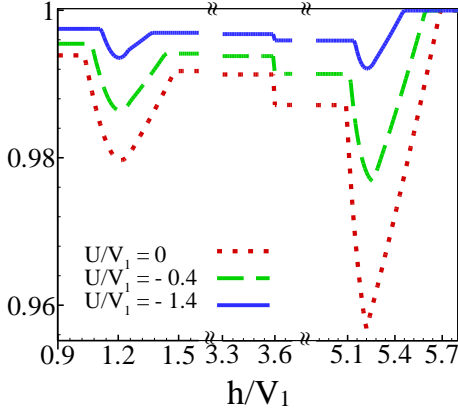


FIG. 4. The order parameter Q^z versus magnetic field for different values of on-site interaction, at $V_2/V_1 = 0.6$ and $J/V_1 = 0.14$.

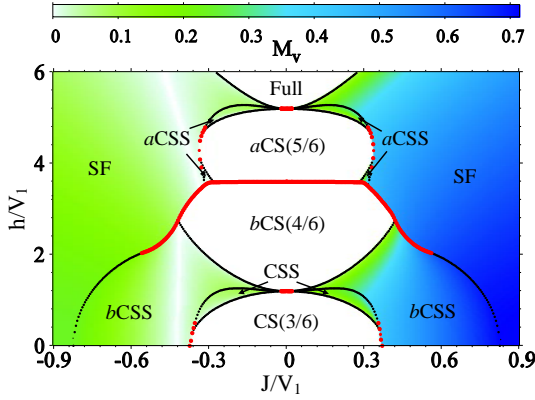


FIG. 5. (Color online) Ground state phase diagram of the iBH mixture for $V_2/V_1 = 0.6$ and $U/V_1 = -1.4$.

trast with the standard $V_1 - V_2$ hardcore Bose Hubbard model^{22,42–44,47,48} on square lattices in which the CSS phase is unstable against quantum fluctuations, and the presence of long range dipole-dipole interactions between hardcore bosons or long range hopping terms are necessary for the stability of the CSS phase^{19,22,46}. Actually, due to the intrinsic difference in the nilpotency condition between a and b bosons ($(a_i^\dagger)^2 = 0$ and $(b_j^\dagger)^3 = 0$, where i and j are nearest neighbor sites) quantum fluctuations are not strong enough to destroy the MI(4/6) and CSS phases. The stability of the CSS phase can be attributed to the large roton-like energy gap in the low energy spin wave excitation spectrum which will be discussed in Sec. V. In this section we will obtain the amount of quantum fluctuations in terms of the number of spin waves and show that the results of CMF- 2×4 are verified by LSW theory.

As the b bosons satisfy the condition $(b_j^\dagger)^3 = 0$, one can put up two b particles on each lattice site. This motivates us to investigate the behavior of the pair superfluid order parameter $\langle (b_j^\dagger)^2 \rangle$ in all phases. In the spin language

this parameter is equivalent to $\frac{1}{2} \langle (\tau_j^+)^2 \rangle$. According to our CMF results (not shown) we find that the pair superfluidity order parameter is zero in the whole range of parameter space. This means that although $(b_j^\dagger)^3 = 0$, but no pairing occurs in the system. We have also computed the order parameter $Q^z = \frac{1}{2} \langle (\tau_B^z)^2 + (\tau_D^z)^2 \rangle$ in different phases. Actually, investigation of the behavior of Q^z gives more intuitions on the properties of solid and Mott insulating phases appeared in the phase diagram. This order parameter is almost 1 in all solid and Mott insulating phases (see Fig. 4). This implies that the local Hilbert space basis for b particles is given by the states: $|0\rangle$ and $|2\rangle$, and consequently the effective Hilbert space dimensions for b particles is two. This fact has been already shown in the schematic pictures of solid and Mott insulating phases in the right panel of Fig. 2.

In the presence of the attractive on-site interaction, at $U \neq 0$, although the superfluidity order parameter decreases with increasing the on-site interaction, there is no considerable changes in the nature of the phases in comparison with the cases of $U = 0$ (see Fig. 4 and 5). The attractive on-site interaction between b particles causes these particles prefer to be at the same site to minimize the interaction energy. This leads to the stability of all the phases at larger values of $|J|$, and therefore to the shift of the phases' borders to the larger values of $|J|$ in the presence of U .

V. LINEAR SPIN WAVE THEORY

In this section, utilizing LSW theory we obtain the excitation spectra of the mixed spin model in Eq. (5). From these spectra besides the strength of quantum fluctuations around the MF ground states, one can find the boundaries of the stability of the mean field phases. Furthermore, by investigating the behavior of the low energy spin wave dispersions at phase transitions one can figure out the reason of all first and second order phase transitions. Before starting the spin wave approach we implement a unitary transformation on the spin Hamiltonian in Eq. 5 and perform the following rotations on all σ and τ spins;

$$\begin{pmatrix} \tilde{\sigma}_i^x \\ \tilde{\sigma}_i^y \\ \tilde{\sigma}_i^z \end{pmatrix} = \begin{pmatrix} \cos \theta_i \cos \phi_i & -\cos \theta_i \sin \phi_i & -\sin \theta_i \\ -\sin \phi_i & \cos \phi_i & 0 \\ \sin \theta_i \cos \phi_i & \sin \theta_i \sin \phi_i & \cos \theta_i \end{pmatrix} \begin{pmatrix} \sigma_i^x \\ \sigma_i^y \\ \sigma_i^z \end{pmatrix},$$

$$\begin{pmatrix} \tilde{\tau}_j^x \\ \tilde{\tau}_j^y \\ \tilde{\tau}_j^z \end{pmatrix} = \begin{pmatrix} \cos \vartheta_j \cos \varphi_j & -\cos \vartheta_j \sin \varphi_j & -\sin \vartheta_j \\ -\sin \varphi_j & \cos \varphi_j & 0 \\ \sin \vartheta_j \cos \varphi_j & \sin \vartheta_j \sin \varphi_j & \cos \vartheta_j \end{pmatrix} \begin{pmatrix} \tau_j^x \\ \tau_j^y \\ \tau_j^z \end{pmatrix},$$

where $\cos \theta_i = \langle \sigma_i^z \rangle / \sigma$, $\tan \phi_i = \langle \sigma_i^y \rangle / \langle \sigma_i^x \rangle$, $\cos \vartheta_j = \langle \tau_j^z \rangle / \tau$ and $\tan \varphi_j = \langle \tau_j^y \rangle / \langle \tau_j^x \rangle$. Here, $\langle \dots \rangle$ denotes the expectation value on the MF ground state of the Hamiltonian in Eq. (5). The rotated spin Hamiltonian is expressed in terms of the new bosonic operators \hat{a} , \hat{b} with

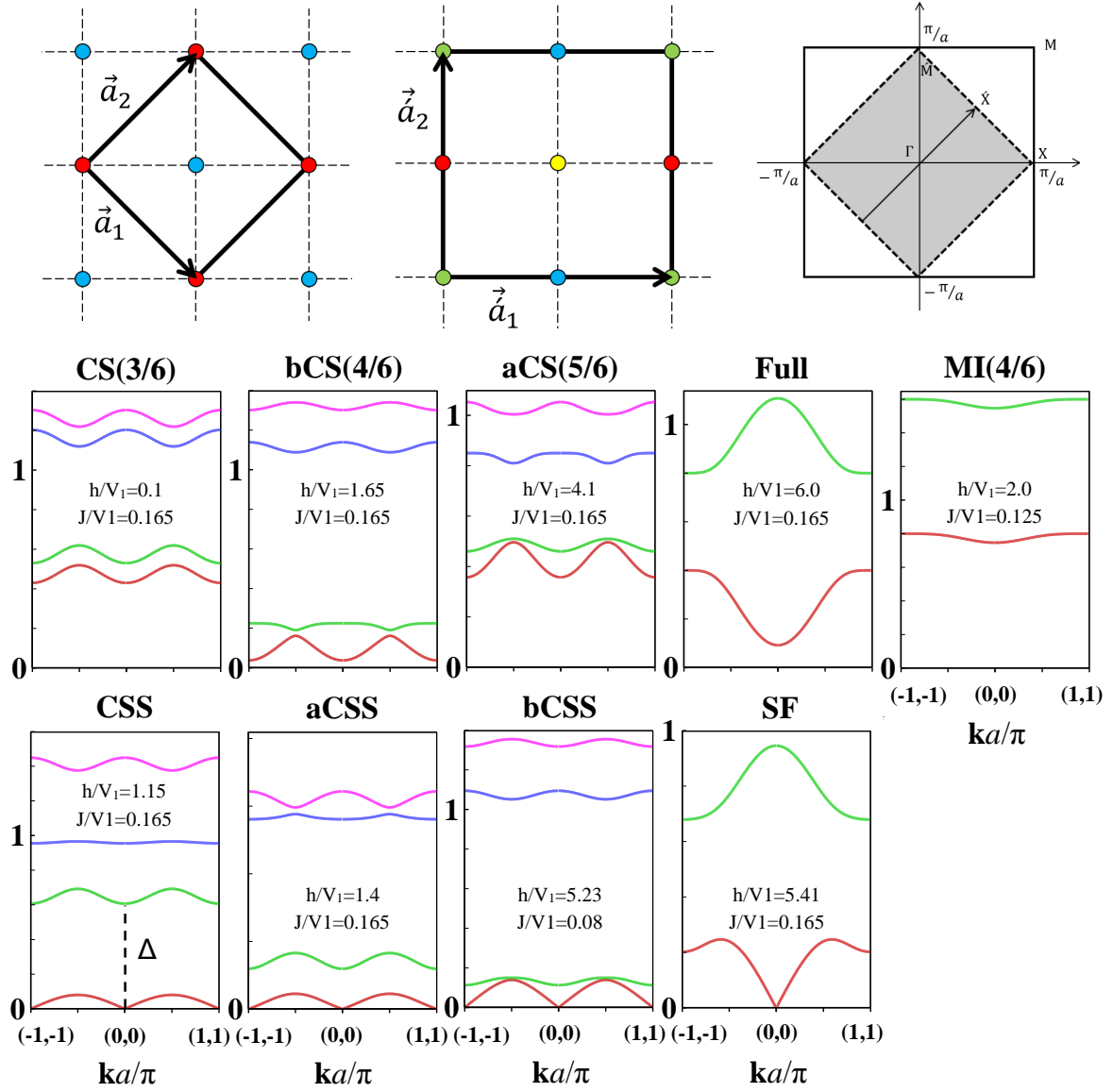


FIG. 6. (Color online) Excitation spectra in various phases of the IBM. Number of excitation modes reflects the number of sublattices in each phase. Top-left: 2D lattice with primitive vectors $\vec{a}_1 = a\hat{x}$ and $\vec{a}_2 = a\hat{y}$ for the MI(4/6), SF and Full phases. Top-center: 2D lattice with primitive vectors $\vec{a}_1 = a(\hat{x} + \hat{y})$ and $\vec{a}_2 = a(-\hat{x} + \hat{y})$ for the solid and supersolid phases where the original lattice symmetry is broken. Top-right: the unfolded and folded Brillouin zones. Middle and bottom: spin wave excitations in all phases in $k_x = k_y$ direction of the unfolded Brillouin zone. The roton gap (Δ) varies in each supersolid phase. All plots are for $V_2/V_1 = 0.6$ except MI(4/6) which is for $V_2/V_1 = 0.2$.

the following Holstein-Primakoff (HP) transformations: and

$$\begin{aligned}
 \tilde{\sigma}_i^z &= \sigma - \hat{a}_i^\dagger \hat{a}_i, \\
 \tilde{\sigma}_i^+ &= \sqrt{2\sigma - \hat{a}_i^\dagger \hat{a}_i} \hat{a}_i \approx \sqrt{2\sigma} \hat{a}_i, \\
 \tilde{\sigma}_i^- &= \hat{a}_i^\dagger \sqrt{2\sigma - \hat{a}_i^\dagger \hat{a}_i} \approx \sqrt{2\sigma} \hat{a}_i^\dagger,
 \end{aligned} \tag{8}$$

$$\begin{aligned}
 \tilde{\tau}_j^z &= \tau - \hat{b}_j^\dagger \hat{b}_j, \\
 \tilde{\tau}_j^+ &= \sqrt{2\tau - \hat{b}_j^\dagger \hat{b}_j} \hat{b}_j \approx \sqrt{2\tau} \hat{b}_j, \\
 \tilde{\tau}_j^- &= \hat{b}_j^\dagger \sqrt{2\tau - \hat{b}_j^\dagger \hat{b}_j} \approx \sqrt{2\tau} \hat{b}_j^\dagger.
 \end{aligned} \tag{9}$$

The spin wave Hamiltonian has the following form;

$$\tilde{H} = E_0 + H', \tag{10}$$

where E_0 is the classical MF energy and H' consists of bilinear terms in HP boson operators. This part yields,

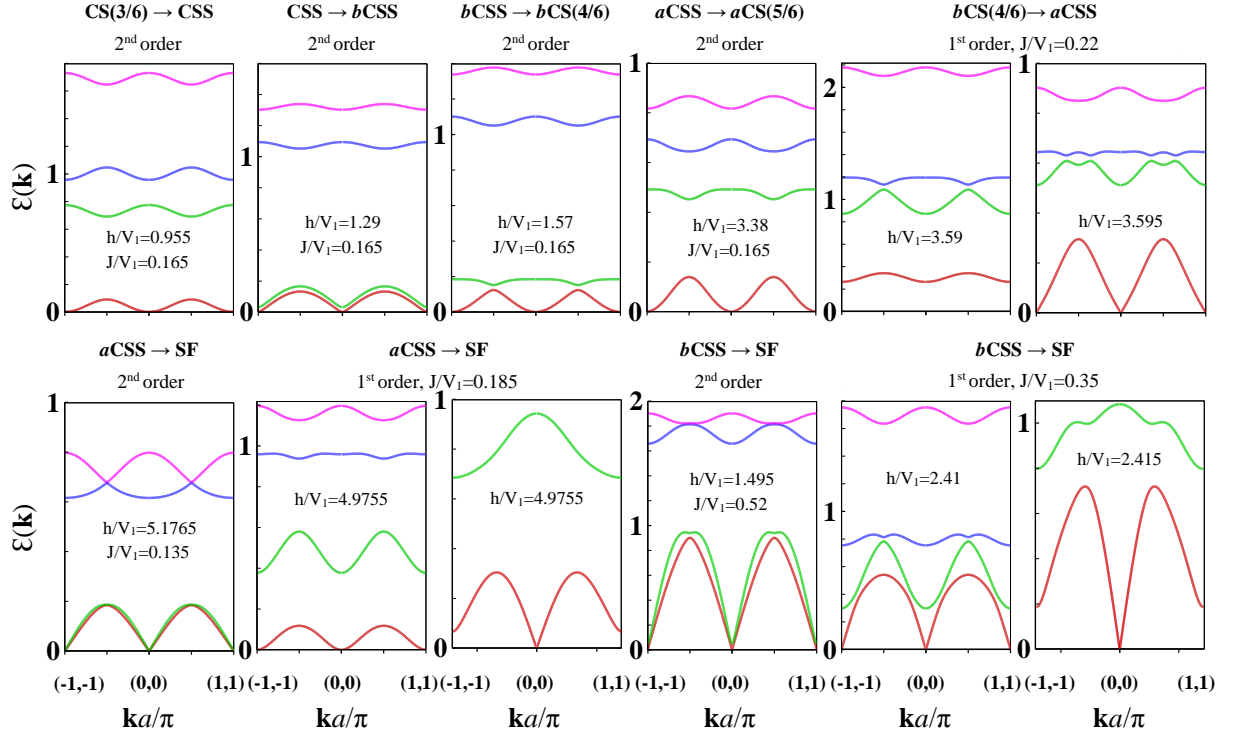


FIG. 7. (Color online) Excitation spectra at various first and second order phase transitions for $V_2/V_1 = 0.6$. In the second order supersolid-solid phase transition (phase transition from $aCSS$ to $aCS(5/6)$, from $bCSS$ to $bCS(4/6)$ and from CSS to $CS(3/6)$) the linear dispersions around $\mathbf{k} = (0,0)$ and $\mathbf{k} = (\pi/a, \pi/a)$ softens to quadratic ones and become gapped in solid phases. In second order phase transitions from $aCSS$ to SF, and from $bCSS$ to SF number of excitations changes and the amount of the roton gap varies continuously. At first order $bCSS$ -SF phase transition the roton gap decreases suddenly. At first order $bCS(4/6)$ - $aCSS$ phase transition the lowest gapped mode abruptly touches zero and the quadratic dispersion changes to a linear one around $\mathbf{k} = (0,0)$ and $\mathbf{k} = (\pi/a, \pi/a)$.

after diagonalization, the excitation spectra in each phase (For the details of diagonalization see the appendix C).

From general symmetry analysis, the off diagonal order parameter manifold has $U(1)$ freedom to rotate the transverse spin order around the magnetic field direction. In the superfluid phase, the $U(1)$ symmetry is spontaneously broken and a gapless Goldstone mode with a roton-like minimum appears in the excitation spectra. The slope of the line connecting the origin of the $\varepsilon - \mathbf{k}$ plane with this minimum is proportional to the critical velocity of the superfluid and the energy of this minimum is the roton energy gap. Upon approaching the transition (second order) from the superfluid side the roton energy and consequently the critical velocity decrease to zero. At the same time the superfluid order parameter remains finite through the supersolid transition. Inside supersolid phases due to the translational symmetry breaking the spatial periodicity is doubled, and the Brillouin zone becomes smaller. So half of the excitation spectrum is folded back to the point $\mathbf{k} = (0,0)$. This second branch acquires a gap, with a quadratic minimum above it, and so the critical velocity will continuously climb back to finite values. The critical velocity in each supersolid phase varies by changing the magnetic field. By comparison of the maximum critical velocities in each

phase we have found out that they satisfy the inequality $v_{aCSS} < v_{bCSS} < v_{CSS}$.

We have plotted in Fig. 6 the spin wave excitation spectra of all phases. Number of excitation modes and their behavior depend on the number of sublattices as well as their longitudinal and transverse magnetizations. According to the Brillouin zone folding, the $k_x = k_y$ direction in the unfolded zone corresponds to the k_x direction in the folded one (See Fig. 6), and so the points $\mathbf{k} = (0,0)$ and $(\pi/a, \pi/a)$ are equivalent. In the SF phase and all the supersolid phases the lower excitation has linear dispersion around the points $\mathbf{k} = (0,0)$. Investigation of the amount of the roton gap in supersolid phases helps us to figure out their stability in the presence of quantum fluctuations. The small roton gap in the $aCSS$ and $bCSS$ phases causes fluctuations annihilate low energy rotons and convert the $aCSS$ and $bCSS$ phases to the CSS one.

In a solid phase there is no Goldstone zero mode and all excitations are gapped. The lowest gapped excitation spectrum has quadratic dispersion (k^2) around $\mathbf{k} = (0,0)$. In $CS(3/6)$ solid and $MI(4/6)$ Mott insulating phases we have found a relation between the excitation energies separation and the magnetic field. In $MI(4/6)$

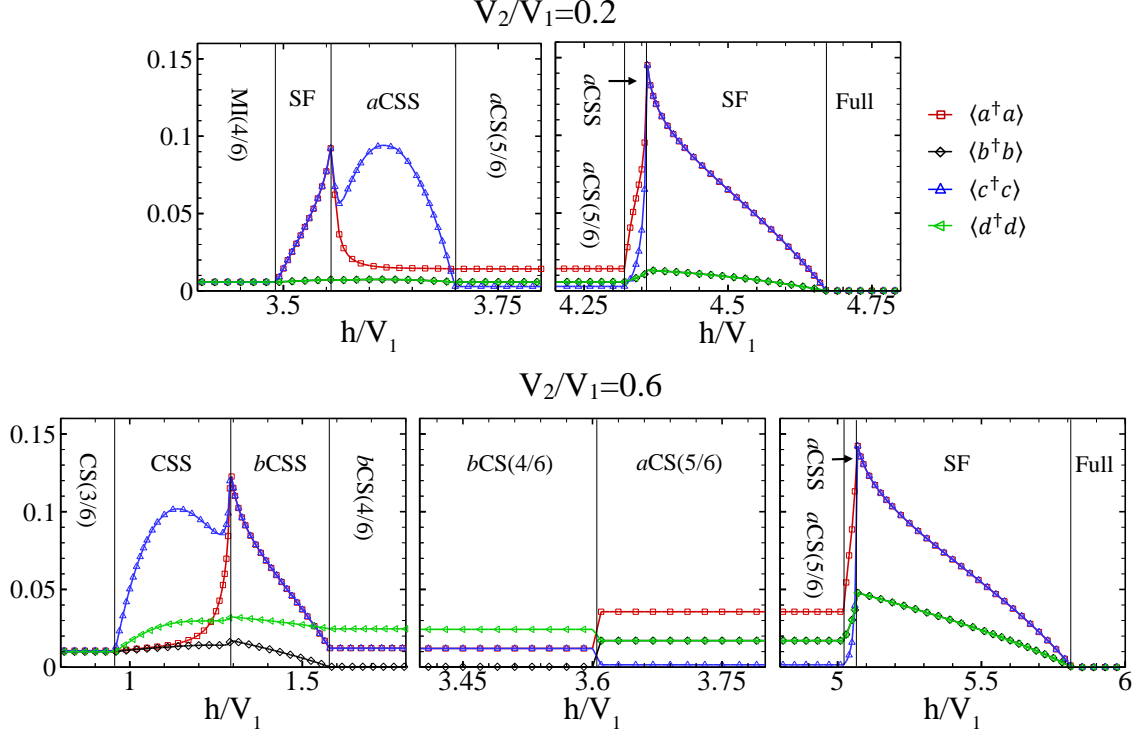


FIG. 8. (Color online) Number of HP bosons around mean field ground state. Top: $V_2/V_1 = 0.2$, at line $J/V_1 = 0.126$. Bottom: $V_2/V_1 = 0.6$, at line $J/V_1 = 0.166$.

phase the two energy bands are related by:

$$\begin{aligned} |\varepsilon^2(\mathbf{k}) - \varepsilon^1(\mathbf{k})| &= -\frac{h}{V_1} + 1.2, & 0 < \frac{h}{V_1} < 1.2, \\ |\varepsilon^2(\mathbf{k}) - \varepsilon^1(\mathbf{k})| &= \frac{h}{V_1} - 1.2, & 1.2 < \frac{h}{V_1}, \end{aligned} \quad (11)$$

and in the CS(3/6) phase, the four energy bands have the relation $|\varepsilon^1(\mathbf{k}) - \varepsilon^2(\mathbf{k})| = |\varepsilon^3(\mathbf{k}) - \varepsilon^4(\mathbf{k})| = \frac{h}{V_1}$, where ε^1 and ε^2 , and ε^3 and ε^4 are the two branches with the same energy behaviors. By increasing magnetic field the two lowest energy bands repel each other causing the energy of the lowest mode decreases and touches zero at $\mathbf{k} = (0, 0)$, when a second order phase transition to the CSS phase occurs in the system.

In order to find out the reason of all first and second order phase transitions in the ground state phase diagram of our IBM, we have also plotted in Fig. 7 the excitation spectra at the phase transition between different phases. The abrupt and smooth changes in the behavior of the low energy excitation modes and the roton gap are the reason of first and second order phase transitions, respectively. In the second order supersolid-solid phase transitions the roton minimum at $\mathbf{k} = (0, 0)$ disappears and the low energy mode softens around this point and becomes gapped in solid phases.

Quantum fluctuations around MF ground state are

given by

$$\begin{aligned} \langle a^\dagger a \rangle &= \langle \sigma_A^z \rangle_{MF} - \langle \sigma_A^z \rangle_{SW}, \\ \langle c^\dagger c \rangle &= \langle \sigma_C^z \rangle_{MF} - \langle \sigma_C^z \rangle_{SW}, \\ \langle b^\dagger b \rangle &= \langle \tau_B^z \rangle_{MF} - \langle \tau_B^z \rangle_{SW}, \\ \langle d^\dagger d \rangle &= \langle \tau_D^z \rangle_{MF} - \langle \tau_D^z \rangle_{SW}, \end{aligned} \quad (12)$$

which are the number of \hat{a} , \hat{b} , \hat{c} , and \hat{d} HP bosons. Here, $\langle \sigma_{A,C}^z \rangle_{MF}$ and $\langle \tau_{B,D}^z \rangle_{MF}$, and $\langle \sigma_{A,C}^z \rangle_{SW}$ and $\langle \tau_{B,D}^z \rangle_{SW}$ are the MF and LSW sublattices' magnetizations, respectively. We have plotted in Fig. 8 the number of HP bosons versus magnetic field, for the two different strengths of frustration $V_2/V_1 = 0.2$ and 0.6 . Larger frustration in the case of $V_2/V_1 = 0.6$ due to the competition between NN and NNN interactions causes stronger quantum fluctuations for $V_2/V_1 = 0.6$ in comparison with the case of $V_2/V_1 = 0.2$. For all strengths of frustration the number of spin waves increases in the vicinity of the transition points which is a result of the strong quantum fluctuations at phase boundaries. Strong quantum fluctuations in the aCSS and bCSS phases is the reason of the converting of these phases to the CSS phase in the CMF- 2×4 results. As we have already mentioned, this instability is also reflected from the behavior of the roton gap in the low energy excitation spectrum.

The small number of \hat{b} and \hat{d} HP bosons in comparison with the number of \hat{a} and \hat{c} is an indication of the weaker quantum fluctuations in the sublattices B and D . The maximum values of $\langle a^\dagger a \rangle (= \langle c^\dagger c \rangle)$ and $\langle b^\dagger b \rangle (= \langle d^\dagger d \rangle)$ in

CSS phases reach respectively about 30 and 5 percent of the classical values of the spin lengths $\sigma = 1/2$ and $\tau = 1$. This means that the prediction for the ground states within CMF- 2×4 theory are reliable. It is worth to compare the amount of quantum fluctuations around the MF ground states of our IBM with the standard Bose Hubbard one. The maximum value of quantum fluctuations in CSS phase of the standard Bose Hubbard is about 77 percent of the classical spin length²² which is much larger than the case of IBM, and cause the CSS phase of the standard Bose Hubbard model, predicted by MF to be unreliable.

VI. FINITE TEMPERATURE PHASE DIAGRAM

At zero temperature, in the superfluidity state each boson is spread out over the entire lattice, with long range phase coherence. At finite temperature, the superfluid density is suppressed and the system undergoes a transition to a thermal insulating phase with varying filling factor. The thermal insulator (TI) is a weak Mott insulator in the sense that it preserves both the translational and the U(1) symmetries. In the presence of temperature, at $T \neq 0$, in the solid phases the plateaus' width on longitudinal magnetization curves decreases gradually by increasing temperature and disappears eventually at a transition temperature which depends on the strength of frustration, the hopping energy J and the magnetic field h . For example, for the strength of $V_2/V_1 = 0.6$ and the hopping energy $J/V_1 = 0.22$, as it is clearly observed from the $T-h$ phase diagram of the IBM (see the top of Fig. 9), the two solid phases $aCS(5/6)$ and $bCS(4/6)$ with constant average number of bosons $5/6$ and $4/6$ survive at low temperature however, by increasing temperature these regions become narrower and finally disappear at the critical temperature $T_{c1} \sim 0.26V_1$ and $T_{c2} \sim 0.37V_1$, where the mixture has a phase transition to the aCS and bCS phases, respectively. In these phases number of particles are not fixed in each unit cell. In the CSS phase, both the diagonal and the off diagonal long range orders tend to be destroyed by thermal fluctuations, however in comparison with the superfluidity order the CS order is more robust. By increasing temperature the superfluidity order parameter vanishes at a transition temperature where the CSS-CS phase transition occurs. (The value of this transition temperature for $V_2/V_1 = 0.6$ is reported in the caption of Fig. 9). The CSS phase persists at finite temperatures comparable with the interaction energies of boson.

In order to see the effects of temperature on the $J-h$ phase diagram of our IBM, we have also plotted in Fig. 9 the $J-h$ phase diagram of the mixture for the frustration parameter $V_2/V_1 = 0.6$, at the finite temperature $T/V_1 = 0.1$. In the presence of temperature, in addition to the ground state phases, several solid orders like CS, aCS and bCS also appear in the phase diagram of

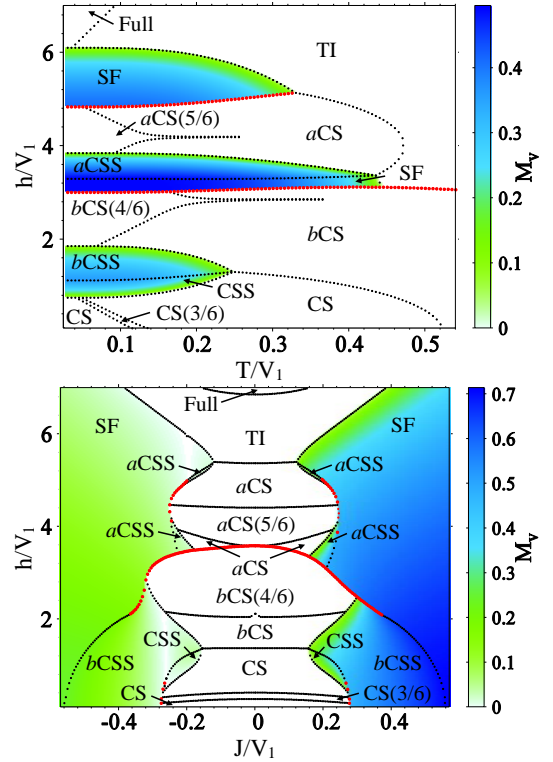


FIG. 9. (Color online) Top: CMF $T-h$ phase diagram of the IBM for $V_2/V_1 = 0.6$ at line $J/V_1 = 0.22$, where all phases emerge by increasing the magnetic field. The SF-TI transition temperature for the two values of magnetic fields $h = 3.22V_1$ and $h = 5.18V_1$ are respectively $0.44V_1$ and $0.32V_1$. The CSS-CS transition temperature at $h/V_1 = 1.30$ is $0.25V_1$. Bottom: CMF $J-h$ phase diagram for the frustration strength $V_2/V_1 = 0.6$ and $T/V_1 = 0.1$.

the mixture. Moreover in the region below the Full solid phase the mixture experiences the TI phase which both the U(1) and the translational symmetries of the original Hamiltonian are preserved. This phase is not seen in the ground state phase diagram and is a result of thermal fluctuations.

VII. SUMMARY AND CONCLUSION

We have introduced an inhomogeneous hardcore bosonic model composed of two kinds of boson with different nilpotency conditions and have shown that the model is an appropriate ground for searching various supersolid orders. By generalizing the cluster mean field theory to the IBM, we have studied both the ground state and the temperature phase diagram of the model on a 2D square lattice. We have found that in addition to the superfluidity phase, various kinds of solid and supersolid emerge in the phase diagram of the inhomogeneous mixture. We have also found that for small strengths of frustration the system possesses a Mott insulating state which preserves both the U(1) and the translational sym-

metries of the Hamiltonian. In order to see the effects of quantum fluctuations on the stability of the ground state phases, we have obtained the diagonal and off diagonal order parameters using the cluster mean field theory with larger clusters. Furthermore, using linear spin wave theory we have studied the behaviors of spin wave excitations and the amount of quantum fluctuations around the mean field ground state to see the stability of the ground state phases of the model. We have demonstrated that in contrast with the standard Bose Hubbard model in which dipole-dipole interactions or long range hoppings are necessary to have an stable checkerboard supersolid phase, our inhomogeneous bosonic mixture with nearest and next nearest neighbor interaction possesses the checkerboard supersolid phase. This stability is attributed to the difference in the nilpotency conditions between a and b bosons.

We have also studied the behavior of the excitation energies in each phase to get more insights on the ground state phases of the model. The excitation modes of the solid phases are gapped and the lowest energy mode has quadratic dispersion around the ordering vectors $\mathbf{k} = (0, 0)$. All the supersolids and also the superfluid, however, possess a gapless Goldstone mode with linear dispersion around this ordering vector. The appearance of this zero mode is a result of the $U(1)$ symmetry breaking due to the superfluidity long range order.

We have also investigated the behavior of the excitation energies around all phase transition points to figure out the reason of first and second order phase transitions. We found out that the abrupt and smooth changes in the behavior of the low energy excitation modes and the roton gap responsible of all first and second order phase transitions, respectively. For example, softening of the linear gapless mode which is accompanied by vanishing of the roton minimum at $\mathbf{k} = (0, 0)$, results the second order supersolid-solid phase transitions.

We have finally investigated the effects of thermal fluctuations on the stability of the ground state phases at finite temperature. We have found that at non-zero temperature, in addition to the ground state phase, other various phases also emerge in the temperature phase diagram. We have shown that the checkerboard supersolid order can persist at finite temperatures comparable with the interaction energies of bosons.

Study of the thermodynamic and magnetocaloric properties of our IBM, and also quantum phase diagram of the mixture on a square lattice with added intra-component interaction are left for the future works.

ACKNOWLEDGMENTS

The authors would like to thank Stefan Wessel for insightful comments on the manuscript. We also thank Marcello Dalmonte for reading the manuscript and introducing some references. Useful discussions with Rosario Fazio, Alexander Nersesyan, Sebastiano Pilati and San-

dro Sorella are acknowledged. JA also thanks ICTP where the initial form of this paper for submission was prepared.

Appendix A: Origin of the IBM Hamiltonian

In this appendix we will explain how the IBM Hamiltonian introduced in Eq. (1), originates from an standard two-orbital Bose-Hubbard model⁵⁶. Let us consider a bipartite model of hard core bosons including two kinds of bosons: a single orbital boson a and a two-orbital boson b_α ($\alpha = \{1, 2\}$), interacting via the Hamiltonian:

$$\begin{aligned} H_{2B} = & -t \sum_{\langle i,j \rangle, \alpha} (a_i^\dagger b_{\alpha j} + h.c.) + U \sum_i n_{1i} n_{2i} \\ & + V_1 \sum_{\langle i,j \rangle} n_i^a (n_j - 1) \\ & + V_2 \sum_{\langle\langle i,j \rangle\rangle} [n_i^a n_j^a + (n_i - 1)(n_j - 1)] \\ & - \sum_i (\mu^a n_i^a + \mu^b n_i), \end{aligned} \quad (A1)$$

where, $n_i^a = a_i^\dagger a_i$ and $n_i = n_{1i} + n_{2i}$ with $n_{\alpha i} = b_{\alpha i}^\dagger b_{\alpha i}$. The local Hilbert space of this bipartite system is a product of the local Hilbert spaces of the subsystems I and II. The dimension of the local Hilbert space of the subsystem I is $D_I = 2$, since per lattice site i we can only have the states $\{|0\rangle_I, a_i^\dagger |0\rangle_I\}$ where, $|0\rangle_I$ is the vacuum state in subsystem I. The dimension of the local Hilbert space of the subsystem II is $D_{II} = 4$, since the states per lattice site j are $\{|0, 0\rangle_{II}, b_{1j}^\dagger |0, 0\rangle_{II}, b_{2j}^\dagger |0, 0\rangle_{II}, b_{1j}^\dagger b_{2j}^\dagger |0, 0\rangle_{II}\}$ where $|0, 0\rangle_{II}$ is the vacuum state in subsystem II.

By defining the following new operators:

$$\tilde{b}_j^\dagger = \frac{1}{\sqrt{2}}(b_{1j}^\dagger - b_{2j}^\dagger), \quad b_j^\dagger = \frac{1}{\sqrt{2}}(b_{1j}^\dagger + b_{2j}^\dagger), \quad (A2)$$

and applying them to the vacuum state $|0, 0\rangle_{II}$ one can get the following antisymmetric and symmetric states:

$$\begin{aligned} |\tilde{\Psi}_j\rangle &= \tilde{b}_j^\dagger |0, 0\rangle_{II} = \frac{1}{\sqrt{2}}(|1, 0\rangle - |0, 1\rangle), \\ |\Psi_j\rangle &= \{ |0, 0\rangle_{II}, b_j^\dagger |0, 0\rangle_{II}, b_j^\dagger b_j^\dagger |0, 0\rangle_{II} \} \\ &= \{ |0, 0\rangle, \frac{1}{\sqrt{2}}(|1, 0\rangle + |0, 1\rangle), |1, 1\rangle \}. \end{aligned} \quad (A3)$$

These states generate another basis for the local Hilbert space of the subsystem II with $D_{II} = 4$ ($n_j = \tilde{b}_j^\dagger \tilde{b}_j + b_j^\dagger b_j$). By writing the Hamiltonian (A1) in terms of the above symmetric and antisymmetric operators, the Hamiltonian decouples into two symmetric and antisymmetric parts, which would be a very helpful step for studying the ground state properties of the model. Before doing this step, some remarks on the local algebra of these operators are in order. Following we will show that the local

algebra satisfied by \tilde{b}_j^\dagger and b_j^\dagger is not the same as the one satisfied by b_{1j}^\dagger and b_{2j}^\dagger .

Let us label the symmetric states as $\{|0\rangle, |1\rangle, |2\rangle\} \equiv \{|0, 0\rangle_{II}, b^\dagger|0, 0\rangle_{II}, b^\dagger b^\dagger|0, 0\rangle_{II}\}$. Action of the operators b^\dagger , b and n^b on these states leads to the following relations:

$$\begin{aligned} b^\dagger|0\rangle &= |1\rangle, & b|0\rangle &= 0, & n^b|0\rangle &= 0, \\ b^\dagger|1\rangle &= |2\rangle, & b|1\rangle &= |0\rangle, & n^b|1\rangle &= |1\rangle, \\ b^\dagger|2\rangle &= 0, & b|2\rangle &= |1\rangle, & n^b|2\rangle &= 2|2\rangle. \end{aligned} \quad (\text{A4})$$

From the above relations one can conclude that the states $|0\rangle$, $|1\rangle$ and $|2\rangle$, respectively contain 0, 1 and 2 numbers of b particles, and n^b is the number operator of b -particles. Moreover the action of the antisymmetric operators \tilde{b}^\dagger , \tilde{b} on the antisymmetric state is given by

$$\tilde{b}^\dagger|\tilde{\Psi}\rangle = -|2\rangle, \quad \tilde{b}|\tilde{\Psi}\rangle = |0\rangle. \quad (\text{A5})$$

Writing down the operators b^\dagger , b , n^b , \tilde{b}^\dagger , and \tilde{b} in terms of the symmetric and antisymmetric states as:

$$\begin{aligned} b^\dagger &= |1\rangle\langle 0| + |2\rangle\langle 1|, & b &= |0\rangle\langle 1| + |1\rangle\langle 2|, \\ n^b &= |\tilde{\Psi}\rangle\langle \tilde{\Psi}| + |1\rangle\langle 1| + 2|2\rangle\langle 2|, \end{aligned} \quad (\text{A6})$$

and

$$\tilde{b}^\dagger = |\tilde{\Psi}\rangle\langle 0| - |2\rangle\langle \tilde{\Psi}|, \quad \tilde{b} = |0\rangle\langle \tilde{\Psi}| - |\tilde{\Psi}\rangle\langle 2|, \quad (\text{A7})$$

we can obtain the following unusual commutation relations:

$$\begin{aligned} [b, b] &= [b^\dagger, b^\dagger] = 0, \\ [b, b^\dagger] &= |0\rangle\langle 0| - |2\rangle\langle 2| = \mathbf{1} - n^b, \\ [n^b, b^\dagger] &= |1\rangle\langle 0| + |2\rangle\langle 1| = b^\dagger, \end{aligned}$$

where $\mathbf{1}$ is the identity matrix for the subsystem II which is written as $\mathbf{1} = |0\rangle\langle 0| + |1\rangle\langle 1| + |2\rangle\langle 2| + |\tilde{\Psi}\rangle\langle \tilde{\Psi}|$. Also in the subsystem I we have:

$$a^\dagger = |1\rangle_I\langle 0|_I, \quad a = |0\rangle_I\langle 1|_I, \quad n^a = |1\rangle_I\langle 1|_I \quad (\text{A8})$$

Now let us go back to the Hamiltonian (A1). Substituting the transformations (A2) into the Hamiltonian (A1), and then using the relations (A6), (A7), and (A8), the Hamiltonian is transformed to (apart from a constant):

$$\begin{aligned} H &= -\sqrt{2}t \sum_{\langle i,j \rangle} (a_i^\dagger b_j + h.c.) + \frac{U}{2} \sum_i n_i^b (n_i^b - 1) \\ &+ V_1 \sum_{\langle i,j \rangle} n_i^a (n_j^b - 1) \\ &+ V_2 \sum_{\langle\langle i,j \rangle\rangle} (n_i^a n_j^a + (n_i^b - 1)(n_j^b - 1)) \\ &- \sum_i (\mu^a n_i^a + \mu^b n_i^b). \end{aligned} \quad (\text{A9})$$

Using the following rescalings

$$\begin{aligned} \sqrt{2}t &\rightarrow t, \quad \frac{U}{2} \rightarrow U, \quad V_1 \rightarrow V_1, \quad V_2 \rightarrow V_2, \\ \mu^a &\rightarrow \mu^a + 4V_1, \quad \mu^b \rightarrow \mu^b + 2U + 8V_2 \end{aligned} \quad (\text{A10})$$

the Hamiltonian (A9) is simplified to:

$$\begin{aligned} H &= -t \sum_{\langle i,j \rangle} (a_i^\dagger b_j + h.c.) + U \sum_i n_i^b n_i^b \\ &+ V_1 \sum_{\langle i,j \rangle} n_i^a n_j^b + V_2 \sum_{\langle\langle i,j \rangle\rangle} (n_i^a n_j^a + n_i^b n_j^b) \\ &- \sum_i (\mu^a n_i^a + \mu^b n_i^b), \end{aligned} \quad (\text{A11})$$

which is the Hamiltonian we have introduced in Eq. (1) of the manuscript. As it is clearly seen the resulted Hamiltonian is obtained in terms of the symmetric operators b^\dagger and b , which means that the local Hilbert space dimension of the subsystem II is effectively $D_s = 3$. As the dimension of the symmetric space is 3 we have employed a simple boson-spin transformations and mapped this subsystem to a system of spin one.

Appendix B: Generalized boson-spin transformations for b bosons

In this appendix we explain briefly how the uncommon nilpotency condition of the b bosons and the fractional exclusion statistics in Eq. 2 lead to the boson-spin mapping of b bosons in Eq. 4. From the commutation relations in Eq. 2, we find that: 1) the number operator of b bosons possesses the relation $(\hat{n}_i^b)^\dagger = \hat{n}_i^b$ and 2) the number operator of b bosons is not equal to $b^\dagger b$, i.e. $\hat{n}_i^b \neq b_i^\dagger b_i$. Actually, due to the non-canonical statistics this kind of bosons are different from the canonical one, and the action of the creation(annihilation) operator $b^\dagger(b)$ on the state $|n_b\rangle$ does not lead to $\sqrt{n_b}|n_b + 1\rangle$ ($\sqrt{n_b}|n_b - 1\rangle$).

As the local space of the b particle is isomorphic with the Hilbert space of a spin 1, employing the following correspondence of boson-spin basis

$$|0\rangle \rightarrow |1, -1\rangle, \quad |1\rangle \rightarrow |1, 0\rangle, \quad |2\rangle \rightarrow |1, +1\rangle, \quad (\text{B1})$$

and

$$\tau^+ |1, -1\rangle = \sqrt{2}|1, 0\rangle, \quad \tau^+ |1, 0\rangle = \sqrt{2}|1, 2\rangle, \quad \tau^+ |1, 2\rangle = 0, \quad (\text{B2})$$

we find the following relations:

$$\tau^z = n^b - 1, \quad \tau^+ = \alpha b^\dagger, \quad (\text{B3})$$

where the coefficient α is readily obtained as follows:

$$\begin{aligned} \tau^+ |1, -1\rangle &= \sqrt{2}|1, 0\rangle, \\ \rightarrow \tau^+ &= \sqrt{2}b^\dagger, \quad \tau^- = \sqrt{2}b. \end{aligned} \quad (\text{B4})$$

These kinds of mapping between fractional hard core bosons and spin operators are usually employed for different standard and non-standard boson Hamiltonian which could be seen in Ref. [56]

Appendix C: Diagonalization of the spin wave Hamiltonian

In order to diagonalize the bilinear part of the spin wave Hamiltonian H' in Eq. (10), the first step in a standard approach, is definition of a Fourier transformation for boson operators \hat{a}_i and \hat{b}_i . Before going to this step, we notice that since the phases: MI(4/6), SF and Full preserve the translational symmetry of the original Hamiltonian the classical background has a two-sublattice structure and the excitations of these phases are achieved by defining the two HP bosons: \hat{a} and \hat{b} . However, in other solid and supersolid phases, according to the translational symmetry breaking, the classical background has a four-sublattice structure and more HP bosons should be employed to attain the excitation spectra of these phases. In this respect, we consider a general background and divide the subsystem with spin σ to two sublattices with bosons \hat{a} and \hat{c} , and the subsystem with spin τ to two sublattices with bosons \hat{b} and \hat{d} . Defining the primitive vectors as in the top-center of Fig. 6 and utilizing the following Fourier transformations;

$$\hat{a}_j = \frac{1}{\sqrt{N/2}} \sum_{\mathbf{k}} e^{-i\mathbf{k} \cdot \mathbf{r}_j} \hat{a}_{\mathbf{k}}, \quad \hat{c}_j = \frac{1}{\sqrt{N/2}} \sum_{\mathbf{k}} e^{-i\mathbf{k} \cdot \mathbf{r}_j} \hat{c}_{\mathbf{k}},$$

$$\hat{b}_j = \frac{1}{\sqrt{N/2}} \sum_{\mathbf{k}} e^{-i\mathbf{k} \cdot \mathbf{r}_j} \hat{b}_{\mathbf{k}}, \quad \hat{d}_j = \frac{1}{\sqrt{N/2}} \sum_{\mathbf{k}} e^{-i\mathbf{k} \cdot \mathbf{r}_j} \hat{d}_{\mathbf{k}},$$

where $N/2$ is the number of each HP boson, the bilinear Hamiltonian is readily obtained as:

$$H' = \sum_{\mathbf{k}} \psi_{\mathbf{k}}^\dagger H_{\mathbf{k}} \psi_{\mathbf{k}},$$

with $\psi_{\mathbf{k}}$, the following 8-component vector:

$$\psi_{\mathbf{k}}^\dagger = (\hat{a}_{\mathbf{k}}^\dagger \quad \hat{b}_{\mathbf{k}}^\dagger \quad \hat{c}_{\mathbf{k}}^\dagger \quad \hat{d}_{\mathbf{k}}^\dagger \quad \hat{a}_{-\mathbf{k}} \quad \hat{b}_{-\mathbf{k}} \quad \hat{c}_{-\mathbf{k}} \quad \hat{d}_{-\mathbf{k}}),$$

and

$$H_{\mathbf{k}} = \begin{pmatrix} A & B \\ B^* & A^* \end{pmatrix}, \quad (C1)$$

where A and B are two 4-square matrices with complex functions. The general forms of the matrices A and B are given by

$$A = \begin{pmatrix} \alpha_{11} & \alpha_2^* & \alpha_9 & \alpha_6^* \\ \alpha_2 & \alpha_{12} & \alpha_8 & \alpha_{10} \\ \alpha_9 & \alpha_8^* & \alpha_{13} & \alpha_4^* \\ \alpha_6 & \alpha_{10} & \alpha_4 & \alpha_{14} \end{pmatrix}, \quad B = \begin{pmatrix} 0 & \alpha_1^* & \alpha_9 & \alpha_5^* \\ \alpha_1^* & 0 & \alpha_7^* & \alpha_{10} \\ \alpha_9 & \alpha_7^* & 0 & \alpha_3^* \\ \alpha_5^* & \alpha_{10} & \alpha_3^* & 0 \end{pmatrix},$$

where

$$\begin{aligned} \alpha_1 &= 2w_{ab}^{11} \cos(k_x a'/2), & \alpha_2 &= 2w_{ab}^{12} \cos(k_x a'/2), \\ \alpha_3 &= 2w_{cd}^{11} \cos(k_x a'/2), & \alpha_4 &= 2w_{cd}^{12} \cos(k_x a'/2), \\ \alpha_5 &= 2w_{ad}^{11} \cos(k_y a'/2), & \alpha_6 &= 2w_{ad}^{12} \cos(k_y a'/2), \\ \alpha_7 &= 2w_{cb}^{11} \cos(k_y a'/2), & \alpha_8 &= 2w_{cb}^{12} \cos(k_y a'/2), \\ \alpha_9 &= 4V_2 g_{ac}^1 \cos(k_x a'/2) \cos(k_y a'/2), \\ \alpha_{10} &= 4V_2 g_{bd}^1 \cos(k_x a'/2) \cos(k_y a'/2), \\ \alpha_{11} &= 2(w_{ab}^{23} + w_{ad}^{23}) + 4V_2 g_{ac}^2 - h e_a, \\ \alpha_{12} &= 2(w_{ab}^{34} + w_{cb}^{34}) + 4V_2 g_{bd}^2 - h e_b, \\ \alpha_{13} &= 2(w_{cb}^{23} + w_{cd}^{23}) + 4V_2 g_{ac}^3 - h e_c, \\ \alpha_{14} &= 2(w_{ad}^{34} + w_{cd}^{34}) + 4V_2 g_{bd}^3 - h e_d, \end{aligned} \quad (C2)$$

with

$$w_{mn}^{\alpha\beta} = V_1 g_{mn}^\alpha - J f_{mn}^\beta. \quad (C3)$$

Here, a' is the length of the primitive vectors shown in the top-center of Fig. 6, α and β are 1, 2, 3, 4 and m and n are the sublattices label: a, b, c and d . The coefficients f_{mn}^β , g_{mn}^α and e_m are given in terms of θ_m, θ_n and ϕ_m, ϕ_n as follows:

$$\begin{aligned} f_{mn}^1 &= \sqrt{S_m S_n} ((\cos \theta_m \cos \theta_n - 1) \cos(\phi_m - \phi_n), \\ &\quad + i \sin(\phi_m - \phi_n) (\cos \theta_n - \cos \theta_m)), \\ f_{mn}^2 &= \sqrt{S_m S_n} ((\cos \theta_m \cos \theta_n + 1) \cos(\phi_m - \phi_n), \\ &\quad + i \sin(\phi_m - \phi_n) (\cos \theta_n + \cos \theta_m)), \\ f_{mn}^3 &= -2S_n \sin \theta_m \sin \theta_n \cos(\phi_m - \phi_n), \\ f_{mn}^4 &= -2S_m \sin \theta_m \sin \theta_n \cos(\phi_m - \phi_n), \\ g_{mn}^1 &= \frac{1}{2} \sqrt{S_m S_n} \sin \theta_m \sin \theta_n, \\ g_{mn}^2 &= -S_n \cos \theta_m \cos \theta_n, \\ g_{mn}^3 &= -S_m \cos \theta_m \cos \theta_n, \\ e_m &= -\cos \theta_m, \end{aligned} \quad (C4)$$

where S_m and S_n are the spins of sublattices m and n , respectively. Performing a paraunitary transformation T , the Hamiltonian $H_{\mathbf{k}}$ in Eq. (C1) is diagonalized as:

$$\psi_{\mathbf{k}}^\dagger H_{\mathbf{k}} \psi_{\mathbf{k}} = \psi_{\mathbf{k}}^\dagger T^\dagger (T^\dagger)^{-1} H_{\mathbf{k}} T^{-1} T \psi_{\mathbf{k}} = \Psi_{\mathbf{k}}^\dagger \mathcal{E}_{\mathbf{k}} \Psi_{\mathbf{k}},$$

where $\mathcal{E}_{\mathbf{k}}$ is the para-diagonalized matrix containing the excitation energies and $\Psi_{\mathbf{k}} = T \psi_{\mathbf{k}}$ is a para-vector of new bosonic operators. The paraunitary transformation satisfies the following relations

$$T \hat{I} T^\dagger = \hat{I}, \quad T^\dagger \hat{I} T = \hat{I}, \quad T^\dagger \hat{I} = \hat{I} T^{-1}, \quad (C5)$$

with

$$\hat{I}_{8 \times 8} = \begin{pmatrix} I_{4 \times 4} & 0 \\ 0 & -I_{4 \times 4} \end{pmatrix},$$

where $I_{4 \times 4}$ is the 4×4 unitary matrix. In order to obtain the paraunitary transformation T we utilize the following procedure which introduced by Colpa for a positive-definite Hamiltonian⁷². First we write the Hamiltonian

$H_{\mathbf{k}}$ as $H_{\mathbf{k}} = \kappa_{\mathbf{k}}^\dagger \kappa_{\mathbf{k}}$ where the matrix $\kappa_{\mathbf{k}}$ is the Cholesky decomposition of the Hamiltonian. Then, we find the unitary transformation matrix, $v_{\mathbf{k}}$ which diagonalizes the hermitian matrix $\kappa_{\mathbf{k}} \hat{I} \kappa_{\mathbf{k}}^\dagger$ as $\mathcal{L}_{\mathbf{k}} = v_{\mathbf{k}}^\dagger (\kappa_{\mathbf{k}} \hat{I} \kappa_{\mathbf{k}}^\dagger) v_{\mathbf{k}}$. The diagonal matrix $\mathcal{E}_{\mathbf{k}}$ is readily obtained from the relation $\mathcal{E}_{\mathbf{k}} = \hat{I} \mathcal{L}_{\mathbf{k}}$. Finally, by solving the equation $v_{\mathbf{k}} \sqrt{\mathcal{E}_{\mathbf{k}}} = \kappa_{\mathbf{k}} T^{-1}$ row to row, we achieve the paraunitary transformation T .

The above diagonalization procedure is for the general case of four-sublattice structure which is employed for the a CS(5/6), b CS(4/6) and CS(3/6) solid, and for a CSS, b CSS and CSS supersolid phases. For the MI(4/6), SF and Full phases where the translational symmetry in both subsystems is preserved, the MF ground states are given by a two-sublattice structure and the 4×4 matrices A and B are simplified to two 2×2 matrices. Following we will obtain these matrices. Using the Fourier transformations;

$$\hat{a}_j = \frac{1}{\sqrt{N}} \sum_{\mathbf{k}} e^{-i\mathbf{k} \cdot \mathbf{r}_j} \hat{a}_{\mathbf{k}}, \quad \hat{b}_j = \frac{1}{\sqrt{N}} \sum_{\mathbf{k}} e^{-i\mathbf{k} \cdot \mathbf{r}_j} \hat{b}_{\mathbf{k}},$$

where N is the number of each HP boson and \mathbf{r}_j is given in terms of the primitive vectors shown in the top-left of Fig. 6, the bilinear Hamiltonian is readily obtained as:

$$H' = \sum_{\mathbf{k}} \psi_{\mathbf{k}}^\dagger H_{\mathbf{k}} \psi_{\mathbf{k}}.$$

with

$$\psi_{\mathbf{k}}^\dagger = (\hat{a}_{\mathbf{k}}^\dagger \quad \hat{b}_{\mathbf{k}}^\dagger \quad \hat{a}_{-\mathbf{k}} \quad \hat{b}_{-\mathbf{k}}),$$

and

$$H_{\mathbf{k}} = \begin{pmatrix} A & B \\ B^* & A^* \end{pmatrix}, \quad (C6)$$

where A and B are given by

$$A = \begin{pmatrix} \alpha_3 & \alpha_2^* \\ \alpha_2 & \alpha_5 \end{pmatrix}, \quad B = \begin{pmatrix} \alpha_4 & \alpha_1^* \\ \alpha_1^* & \alpha_6 \end{pmatrix},$$

where

$$\begin{aligned} \alpha_1 &= 2w_{ab}^{11} \cos(k_x a/2) \cos(k_y a/2), \\ \alpha_2 &= 2w_{ab}^{12} \cos(k_x a/2) \cos(k_y a/2), \\ \alpha_3 &= 4w_{ab}^{23} - h e_a \\ &\quad + 2V_2 (g_{aa}^2 + g_{aa}^3 + g_{aa}^1 (\cos(k_x a) + \cos(k_y a))), \\ \alpha_4 &= V_2 g_{aa}^1 (\cos(k_x a) + \cos(k_y a)), \\ \alpha_5 &= 4w_{ab}^{34} - h e_b \\ &\quad + 2V_2 (g_{bb}^2 + g_{bb}^3 + g_{bb}^1 (\cos(k_x a) + \cos(k_y a))), \\ \alpha_6 &= V_2 g_{bb}^1 (\cos(k_x a) + \cos(k_y a)). \end{aligned} \quad (C7)$$

* fheydari@iasbs.ac.ir

† jahan@iasbs.ac.ir

- ¹ H. Matsuda and T. Tsuneto, Progress of Theoretical Physics Supplement **46**, 411 (1970).
- ² K.-S. Liu and M. E. Fisher, Journal of Low Temperature Physics **10**, 655 (1973).
- ³ A. Griesmaier, J. Werner, S. Hensler, J. Stuhler, and T. Pfau, Phys. Rev. Lett. **94**, 160401 (2005).
- ⁴ J. Deiglmayr, A. Grochola, M. Repp, K. Mörtlbauer, C. Glück, J. Lange, O. Dulieu, R. Wester, and M. Weidemüller, Phys. Rev. Lett. **101**, 133004 (2008).
- ⁵ K.-K. Ni, S. Ospelkaus, M. H. G. de Miranda, A. Pe'er, B. Neyenhuis, J. J. Zirbel, S. Kotochigova, P. S. Julienne, D. S. Jin, and J. Ye, Science **322**, 231 (2008).
- ⁶ M. Lu, N. Q. Burdick, S. H. Youn, and B. L. Lev, Phys. Rev. Lett. **107**, 190401 (2011).
- ⁷ K. Aikawa, A. Frisch, M. Mark, S. Baier, A. Rietzler, R. Grimm, and F. Ferlaino, Phys. Rev. Lett. **108**, 210401 (2012).
- ⁸ K. Aikawa, D. Akamatsu, M. Hayashi, K. Oasa, J. Kobayashi, P. Naidon, T. Kishimoto, M. Ueda, and S. Inouye, Phys. Rev. Lett. **105**, 203001 (2010).
- ⁹ G. G. Batrouni, F. Hébert, and R. T. Scalettar, Phys. Rev. Lett. **97**, 087209 (2006).
- ¹⁰ P. Sengupta and C. D. Batista, Phys. Rev. Lett. **99**, 217205 (2007).
- ¹¹ L. Mathey, I. Danshita, and C. W. Clark, Phys. Rev. A **79**, 011602 (2009).
- ¹² F. J. Burnell, M. M. Parish, N. R. Cooper, and S. L. Sondhi, Phys. Rev. B **80**, 174519 (2009).
- ¹³ K. Góral, L. Santos, and M. Lewenstein, Phys. Rev. Lett. **88**, 170406 (2002).
- ¹⁴ D. L. Kovrizhin, G. V. Pai, and S. Sinha, EPL (Euro-

- physics Letters) **72**, 162 (2005).
- ¹⁵ P. Sengupta, L. P. Pryadko, F. Alet, M. Troyer, and G. Schmid, Phys. Rev. Lett. **94**, 207202 (2005).
- ¹⁶ V. W. Scarola and S. Das Sarma, Phys. Rev. Lett. **95**, 033003 (2005).
- ¹⁷ S. Yi, T. Li, and C. P. Sun, Phys. Rev. Lett. **98**, 260405 (2007).
- ¹⁸ I. Danshita and C. A. R. Sá de Melo, Phys. Rev. Lett. **103**, 225301 (2009).
- ¹⁹ B. Capogrosso-Sansone, C. Trefzger, M. Lewenstein, P. Zoller, and G. Pupillo, Phys. Rev. Lett. **104**, 125301 (2010).
- ²⁰ I. Danshita and D. Yamamoto, Phys. Rev. A **82**, 013645 (2010).
- ²¹ F. Mila, J. Dorier, and K. P. Schmidt, Progress of Theoretical Physics Supplement **176**, 355 (2008).
- ²² D. Yamamoto, A. Masaki, and I. Danshita, Phys. Rev. B **86**, 054516 (2012).
- ²³ K.-K. Ng and Y.-C. Chen, Physical Review B **77**, 052506 (2008).
- ²⁴ S. Wessel, Phys. Rev. B **75**, 174301 (2007).
- ²⁵ J. Y. Gan, Y. C. Wen, J. Ye, T. Li, S.-J. Yang, and Y. Yu, Phys. Rev. B **75**, 214509 (2007).
- ²⁶ S. Wessel and M. Troyer, Phys. Rev. Lett. **95**, 127205 (2005).
- ²⁷ D. Heidarian and K. Damle, Phys. Rev. Lett. **95**, 127206 (2005).
- ²⁸ R. G. Melko, A. Paramekanti, A. A. Burkov, A. Vishwanath, D. N. Sheng, and L. Balents, Phys. Rev. Lett. **95**, 127207 (2005).
- ²⁹ M. Boninsegni and N. Prokof'ev, Phys. Rev. Lett. **95**, 237204 (2005).
- ³⁰ S. R. Hassan, L. de Medici, and A.-M. S. Tremblay, Phys.

- Rev. B **76**, 144420 (2007).
- ³¹ A. Sen, P. Dutt, K. Damle, and R. Moessner, Phys. Rev. Lett. **100**, 147204 (2008).
 - ³² L. Pollet, J. D. Picon, H. P. Büchler, and M. Troyer, Phys. Rev. Lett. **104**, 125302 (2010).
 - ³³ L. Bonnes and S. Wessel, Phys. Rev. B **84**, 054510 (2011).
 - ³⁴ X.-F. Zhang, R. Dillenschneider, Y. Yu, and S. Eggert, Phys. Rev. B **84**, 174515 (2011).
 - ³⁵ D. Yamamoto, I. Danshita, and C. A. R. Sá de Melo, Phys. Rev. A **85**, 021601 (2012).
 - ³⁶ S. V. Isakov, S. Wessel, R. G. Melko, K. Sengupta, and Y. B. Kim, Phys. Rev. Lett. **97**, 147202 (2006).
 - ³⁷ K.-K. Ng and T. K. Lee, Phys. Rev. Lett. **97**, 127204 (2006).
 - ³⁸ C. Trefzger, C. Menotti, and M. Lewenstein, Phys. Rev. Lett. **103**, 035304 (2009).
 - ³⁹ K. Yamamoto, S. Todo, and S. Miyashita, Phys. Rev. B **79**, 094503 (2009).
 - ⁴⁰ B. Xi, F. Ye, W. Chen, F. Zhang, and G. Su, Phys. Rev. B **84**, 054512 (2011).
 - ⁴¹ T. Ohgoe, T. Suzuki, and N. Kawashima, Phys. Rev. Lett. **108**, 185302 (2012).
 - ⁴² G. G. Batrouni and R. T. Scalettar, Phys. Rev. Lett. **84**, 1599 (2000).
 - ⁴³ G. Schmid, S. Todo, M. Troyer, and A. Dorneich, Physical review letters **88**, 167208 (2002).
 - ⁴⁴ F. Hebert, G. G. Batrouni, R. Scalettar, G. Schmid, M. Troyer, and A. Dorneich, Physical Review B **65**, 014513 (2001).
 - ⁴⁵ N. G. Zhang and C. L. Henley, Phys. Rev. B **68**, 014506 (2003).
 - ⁴⁶ T. Ohgoe, T. Suzuki, and N. Kawashima, Journal of the Physical Society of Japan **80**, 113001 (2011).
 - ⁴⁷ R. T. Scalettar, G. G. Batrouni, A. P. Kampf, and G. T. Zimanyi, Phys. Rev. B **51**, 8467 (1995).
 - ⁴⁸ L. Dang, M. Boninsegni, and L. Pollet, Physical Review B **78**, 132512 (2008).
 - ⁴⁹ K. P. Schmidt, J. Dorier, A. M. Läuchli, and F. Mila, Phys. Rev. Lett. **100**, 090401 (2008).
 - ⁵⁰ H. P. Büchler and G. Blatter, Phys. Rev. Lett. **91**, 130404 (2003).
 - ⁵¹ I. Titvinidze, M. Snoek, and W. Hofstetter, Phys. Rev. Lett. **100**, 100401 (2008).
 - ⁵² P. P. Orth, D. L. Bergman, and K. Le Hur, Physical Review A **80**, 023624 (2009).
 - ⁵³ A. Hubener, M. Snoek, and W. Hofstetter, Phys. Rev. B **80**, 245109 (2009).
 - ⁵⁴ T. Keilmann, I. Cirac, and T. Roscilde, Phys. Rev. Lett. **102**, 255304 (2009).
 - ⁵⁵ Z. Yan, X. Yang, and S. Wan, Journal of Physics B: Atomic, Molecular and Optical Physics **46**, 055302 (2013).
 - ⁵⁶ C. D. Batista and G. Ortiz, Advances in Physics **53**, 1 (2004).
 - ⁵⁷ M. Aidelsburger, M. Atala, M. Lohse, J. T. Barreiro, B. Paredes, and I. Bloch, Physical review letters **111**, 185301 (2013).
 - ⁵⁸ H. Miyake, G. A. Siviloglou, C. J. Kennedy, W. C. Burton, and W. Ketterle, Physical review letters **111**, 185302 (2013).
 - ⁵⁹ S. Greschner, L. Santos, and T. Vekua, Physical Review A **87**, 033609 (2013).
 - ⁶⁰ N. Y. Yao, C. R. Laumann, A. V. Gorshkov, S. D. Bennett, E. Demler, P. Zoller, and M. D. Lukin, Physical review letters **109**, 266804 (2012).
 - ⁶¹ N. Y. Yao, A. V. Gorshkov, C. R. Laumann, A. M. Läuchli, J. Ye, and M. D. Lukin, Physical review letters **110**, 185302 (2013).
 - ⁶² M. Aguado, G. K. Brennen, F. Verstraete, and J. I. Cirac, Phys. Rev. Lett. **101**, 260501 (2008).
 - ⁶³ T. Keilmann, S. Lanzmich, I. McCulloch, and M. Roncaglia, arXiv preprint arXiv:1009.2036 (2010).
 - ⁶⁴ C. Sträter, S. C. L. Srivastava, and A. Eckardt, Phys. Rev. Lett. **117**, 205303 (2016).
 - ⁶⁵ J. Arcila-Forero, R. Franco, and J. Silva-Valencia, Phys. Rev. A **94**, 013611 (2016).
 - ⁶⁶ M. Atala, M. Aidelsburger, M. Lohse, J. T. Barreiro, B. Paredes, and I. Bloch, Nature Physics **10**, 588 (2014).
 - ⁶⁷ S. Greschner and L. Santos, Physical review letters **115**, 053002 (2015).
 - ⁶⁸ A. Daley, J. Taylor, S. Diehl, M. Baranov, and P. Zoller, Physical review letters **102**, 040402 (2009).
 - ⁶⁹ T. Matsubara and H. Matsuda, Progress of Theoretical Physics **16**, 569 (1956).
 - ⁷⁰ D. Yamamoto, Physical Review B **79**, 144427 (2009).
 - ⁷¹ T. Oguchi, Progress of Theoretical Physics **13**, 148 (1955).
 - ⁷² J. Colpa, Physica A: Statistical Mechanics and its Applications **93**, 327 (1978).